Geophysical Research Letters

RESEARCH LETTER
10.1029/2018GL079122

Key Points:
- Interannual variability in ocean heat content is driven by both air-sea heat fluxes and ocean heat flux divergence
- The oceanic contribution is driven by fluxes through the southern boundary of the study area
- Subtropical-sourced waters are the major contributor to interannual variability in the flux through the southern boundary

Supporting Information:
- Supporting Information S1

Correspondence to:
N. P. Foukal,
nfoukal@whoi.edu

Citation:
Foukal, N. P., & Lozier, M. S. (2018). Examining the origins of ocean heat content variability in the eastern North Atlantic subpolar gyre. *Geophysical Research Letters*, *45*, 11,275–11,283. https://doi.org/10.1029/2018GL079122

Received 6 JUN 2018
Accepted 5 OCT 2018
Accepted article online 10 OCT 2018
Published online 27 OCT 2018

Examining the Origins of Ocean Heat Content Variability in the Eastern North Atlantic Subpolar Gyre

Nicholas P. Foukal[1,2] **and M. Susan Lozier**[1]

[1]Division of Earth and Ocean Sciences, Nicholas School of the Environment, Duke University, Durham, NC, USA, [2]Now at Department of Physical Oceanography, Woods Hole Oceanographic Institution, Woods Hole, MA, USA

Abstract We analyze sources of ocean heat content (OHC) variability in the eastern North Atlantic subpolar gyre from both Eulerian and Lagrangian perspectives within two ocean simulations from 1990 to 2015. Heat budgets reveal that while the OHC seasonal cycle is driven by air-sea fluxes, interannual OHC variability is driven by both air-sea fluxes and the divergence of ocean heat transport, the latter of which is dominated by the oceanic flux through the southern face of the study area. Lagrangian trajectories initialized along the southern face and run backward in time indicate that interannual variability in the subtropical-origin volume flux (i.e., the upper limb of the overturning circulation) drives variability in the temperature flux through the southern face. As such, the heat carried by the imported subtropical waters is an important component of the eastern subpolar gyre heat budget on interannual time scales.

Plain Language Summary The waters off northern Europe, or the eastern portion of the subpolar North Atlantic, have two characteristics that are of interest: (1) they affect the climate of northern Europe and (2) they are potentially predictable on monthly to decadal time scales. In this paper, we analyze the temperature variability of the eastern subpolar North Atlantic by bounding the region by four faces, three in the ocean plus the surface, and calculating the fluxes of heat across each face. We find that the heat fluxes through the surface explain the majority of the seasonal summer warming and winter cooling, but when the average seasonal cycle is removed, the remainder of the temperature variability is explained by a combination of the heat fluxes through the surface and from waters originating in the Gulf Stream. Thus, the classical view of Gulf Stream waters impacting the high-latitude North Atlantic temperature variability is confirmed, though with the important caveat that there are a number of other possible sources of variability (e.g., surface forcing, variability from the western subpolar North Atlantic) that combined exert a larger effect on the temperature variability of the eastern subpolar North Atlantic and cannot be ignored in seasonal to interannual predictions.

1. Introduction

Recent studies have suggested that North Atlantic subpolar gyre (SPG) temperature variability precedes multidecadal variability in the basin-averaged (0–70°N) North Atlantic sea surface temperature (SST), termed the Atlantic Multidecadal Variability (AMV; Buckley et al., 2012; Brown et al., 2016; Delworth et al., 2017; Frajka-Williams et al., 2017, and references therein). Variability in the SPG temperature has been commonly attributed to the import of water from the subtropical gyre (STG) to the SPG as part of the upper limb of the Atlantic Meridional Overturning Circulation (AMOC; Häkkinen & Rhines, 2004; Holliday, 2003; Rahmstorf et al., 2015; Robson et al., 2016; Sutton & Allen, 1997). However, others (Cane et al., 2017; Trenary & DelSole, 2016) have questioned these correlative studies and suggest that a causal link between the AMOC and the AMV has not yet been established. Furthermore, a recent series of papers has proposed two alternative explanations for the AMV that focus on atmospheric forcing: (1) an oceanic red noise response to white noise atmospheric variability (Cane et al., 2017; Clement et al., 2015) and (2) a response to historical external forcings such as aerosols and volcanoes (Bellomo et al., 2017; Murphy et al., 2017). Arguments for either side of this debate—the oceanic and the atmospheric—rely on indirect measurements of the ocean's contribution to temperature variability because historical ocean observations are too sparse to reliably calculate heat fluxes (Roberts et al., 2017). Here we use two ocean circulation models to directly assess the importance of the oceanic heat flux divergence to the heat budget of the eastern SPG.

The mechanism by which the ocean heat flux divergence impacts the SPG temperature variability is also a topic of debate. Häkkinen and Rhines (2004) and Hátún et al. (2005) posit that the size and strength of the

SPG allows more (less) subtropical-sourced waters into the eastern SPG when the gyre is contracted (expanded). But their altimetry-based, Gyre Index continued to decline from 1992 to 2015, despite a distinct reversal from a warming SPG from the 1990s to 2005 to a cooling SPG from 2005 to present, leading Foukal and Lozier (2017) to determine that the gyre dynamics are not connected to the properties of the eastern SPG on interannual time scales. Piecuch et al. (2017) argue that the 2005 reversal was due to a change in the horizontal gyre circulation as measured at 46°N, still implying that the eastern SPG temperature variability arises from variability local to the SPG. In contrast, Robson et al. (2016) suggest that the cooling since 2005 has been due to an AMOC reduction at 40°N, thereby implying that SPG temperature variability is sourced from the subtropics.

Resolution of these Eulerian perspectives requires an understanding of the pathways to the eastern SPG, such as that provided by a Lagrangian perspective. Burkholder and Lozier (2014) use simulated backward trajectories from the eastern SPG to show that 75–80% of the eastern SPG waters from the upper thermocline are supplied from the STG, while only 5–7% originate in the relatively cold western SPG. This result suggests that subtropical waters likely play a role in setting the temperature variability of the eastern SPG. Similarly, Desbruyères et al. (2013, 2015) use simulated backward trajectories to determine that decadal temperature variability in the area between the OVIDE line (spanning Greenland to Portugal) and the Greenland-Iceland-Scotland Ridge is driven by transport anomalies along the OVIDE line and that these transport anomalies are set by the relative proportion of cold SPG-sourced waters and warm STG-sourced waters arriving to the OVIDE line at a given time. Though this result is pertinent to our question on the source regions of SPG temperature variability, the positioning of the OVIDE line across the STG-SPG boundary hinders a direct application of their results to our question. Here we focus on the origins of eastern SPG temperature variability by running Lagrangian trajectories backward in time from a region entirely contained in the SPG and track the pathways that lead to the SPG. In particular, we focus on the eastern SPG as it is the entranceway for subtropical water to enter subpolar latitudes and the SST in this region has been shown to be important to climate predictability (e.g., Årthun et al., 2018; Latif et al., 2006) and marine ecosystems (e.g., Alheit et al., 2017; Hátún et al., 2009).

2. Methods

The Family of Linked Atlantic Modeling Experiments (FLAME; Böning et al., 2006; Biastoch et al., 2008) is a 1/12th degree, fully dynamic ocean circulation model of the North Atlantic (18°S–70°N, 100°W–15°E) and is built on the Modular Ocean Model (MOM) version 2.1 framework (Pacanowski, 1996). FLAME has 45 *z*-coordinate depth levels with spacing ranging from 10 m at the surface to 250 m below 2,000 m and is forced by European Centre for Medium-Range Weather Forecasts climatological surface buoyancy and wind forcing and anomalies from National Centers for Environmental Prediction/National Center for Atmospheric Research (NCEP/NCAR) Reanalysis from 1990 to 2004 (Kalnay, 1996). To account for FLAME's B-grid structure, the Lagrangian particle tracking software was developed specifically for FLAME (Gary et al., 2011).

ECCO version 4 release 3 (hereafter referred to as ECCO) is a global oceanic state estimate using the Massachusetts Institute of Technology (MIT) general circulation model at 1/4–1° nominal resolution and an energetically conserving data assimilation technique (Forget et al., 2015; Fukumori et al., 2017). ECCO has 50 *z*-coordinate depth levels with 10-m spacing at the surface, increasing to 445-m spacing at the bottom. The time period extends from 1992 to 2015 with output at monthly resolution. To recover heat and freshwater budgets from the original model run, ECCO archives (1) variables that describe the model's dynamics (e.g., temperature and salinity fluxes), resolved on the native hourly resolution and averaged to monthly resolution, and (2) snapshots of property fields (potential temperature, salinity, and sea surface height) at the beginning and end of each month, so that temporal derivatives can be calculated over each month (Piecuch, 2017). While ECCO is useful for recreating heat budgets, its relatively coarse spatial resolution and monthly temporal resolution precludes its usefulness for understanding Lagrangian pathways. Thus, for this study ECCO is only used in the heat budget (section 3), while FLAME is used in both the heat budget and Lagrangian analysis (sections 3 and 4).

To validate the use of these models, we compare the ocean heat content (OHC) variability in the eastern SPG from FLAME and ECCO to observations from the Hadley Centre EN4 objective analysis fields (version 4.1.1; Good et al., 2013). Both ECCO and FLAME accurately simulate the observed OHC variability in the eastern

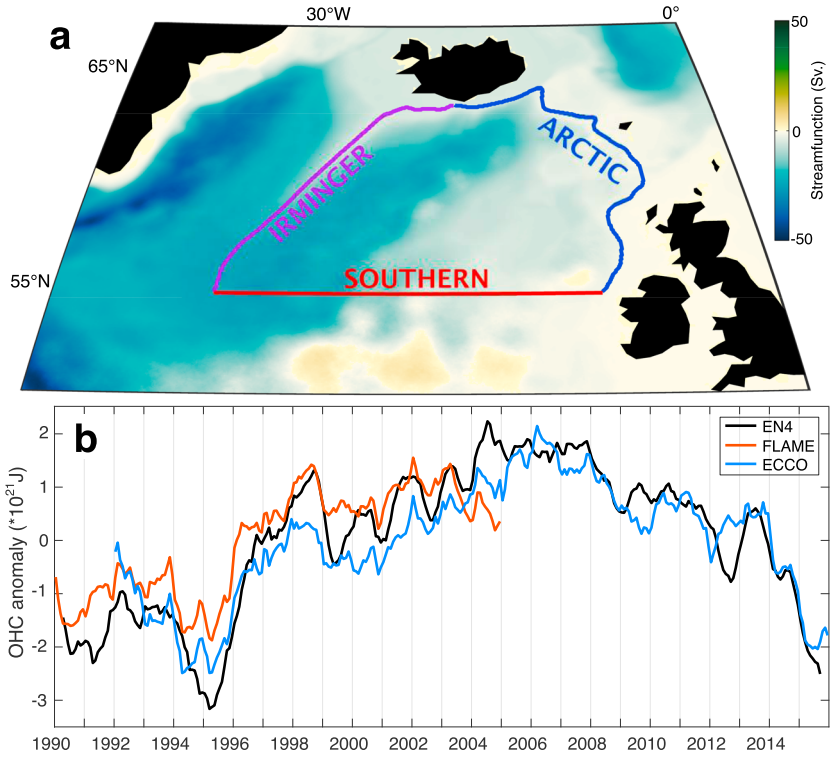

Figure 1. Study area and model validation. (a) Time-averaged barotropic stream function (Sv) from FLAME, with the study area delineated. The study area, with Southern, Arctic, and Irminger faces, is aligned with the 500-m isobath on its eastern and northern edges, the Reykjanes ridge on the western edge, and bounded to the south by 54.5°N. The southern boundary was chosen to remain north of the Charlie Gibbs fracture zone (at 53.5°N), where topographically constrained zonal flow across the mid-Atlantic ridge (Bower et al., 2002) could complicate our calculations. We use the surface-to-bottom water column for the heat budget analysis (section 3) to isolate the ocean heat flux divergence and surface forcing. In the Lagrangian analysis (section 4), trajectories are seeded from the surface to 500 m depth, a vertical extent that captures 96% of the intergyre exchange and 85% of the temperature flux through the Southern face (similar to results from Boccaletti et al. (2005)), while significantly reducing the computational costs of the Lagrangian analysis. (b) Variability in OHC anomalies from 1990 to 2015 in EN4 observations (black, 1990–2015, standard deviation = $1.35*10^{21}$ J), FLAME (orange, 1990–2004, standard deviation = $0.92 * 10^{21}$ J) and ECCO (blue, 1992–2015 standard deviation = $0.97* 10^{21}$ J). the observed EN4 OHC is strongly related to ECCO OHC (explains 76% of EN4 variance, or 85% when 5-month smoothed) and the FLAME OHC (explains 70% of EN4 variance, or 79% when 5-month smoothed). FLAME data are averaged to monthly resolution from three-day resolution for direct comparison.

SPG (Figure 1b). The strong relation between FLAME and EN4 is more noteworthy than that between ECCO and EN4 because ECCO assimilates the same data used for the EN4 product. Furthermore, this strong relationship between the FLAME and EN4 OHC coupled with the fact that FLAME uses realistic surface fluxes suggests that the ocean heat divergence in FLAME is similar to that in the real ocean for our study domain.

In this manuscript, we use two metrics to demonstrate the relation between two variables. When the variables have the same units, we use percent variance explained, defined as

$$\text{Variance of } X \text{ explained by } Y\ (\%) = \ 100*\left[1-\left(\frac{\sigma^2(X-Y)}{\sigma^2(X)}\right)\right]$$

where σ^2 denotes the variance. This method accounts for the magnitude of the variability as well as the variables' covariance through time. If the forcings (e.g., ocean heat divergence and surface fluxes) are not independent, it is possible that the sum of the variances explained will exceed 100%, but the relative importance of the forcings is reflected by this measure. When the two variables do not have the same units (e.g., transport variability measured in Sverdrups, 1 Sv = 10^6 m^3/s, and heat flux measured in petawatts, 1 PW = 10^{15} W), we relate the two through the linear correlation coefficient (r).

Table 1
Components of the Eastern SPG Heat Budget at Monthly Resolution

		Seasonal		Interannual	
		FLAME	ECCO	FLAME	ECCO
OHC tendency	Mean ± stdv. (PW)	0 ± 0.16	0 ± 0.18	0 ± 0.06	0 ± 0.07
Surface	Mean ± stdv. (PW)	−0.10 ± 0.15	−0.09 ± 0.16	0 ± 0.03	0 ± 0.04
	Variance expl. (%)	**90**	**94**	47	**67**
Oceanic convergence	Mean ± stdv. (PW)	0.11 ± 0.05	0.09 ± 0.05	0 ± 0.06	0 ± 0.04
	Variance expl. (%)	16	31	**80**	**68**
Southern	Mean ± stdv. (PW)	0.31 ± 0.05	0.24 ± 0.03	0 ± 0.04	0 ± 0.03
	Variance expl. (%)	**72** (56, 67)	**66** (43, 55)	**83** (76, 76)	**77** (60, 61)
Arctic	Mean ± stdv. (PW)	−0.12 ± 0.02	−0.10 ± 0.02	0 ± 0.02	0 ± 0.02
	Variance expl. (%)	18 (16, 18)	**56** (56, 56)	26 (26, 26)	46 (45, 45)
Irminger	Mean ± stdv. (PW)	−0.09 ± 0.02	−0.02 ± 0.01	0 ± 0.01	0 ± 0.01
	Variance expl. (%)	5 (−5, 3)	12 (12, 9)	11 (−1, −1)	4 (−1, −1)
Residual	Mean ± stdv. (PW)	0 ± 0.01	0 ± 0.01	0 ± 0.01	0 ± 0.01

Note. To close the heat budget in ECCO, in addition to the advective fluxes (shown above), diffusive fluxes (southern = −0.001 ± 0.003 PW, Arctic = −0.012 ± 0.002 PW, Irminger = −0.025 ± 0.005 PW) and a geothermal flux (0.0001 PW, time-invariant) were added to the equation in section 3. Variance explained in the Surface and Oceanic convergence rows refers to the amount of OHC tendency variance explained by each variable, while the Southern, Arctic, and Irminger rows refer to the amount of Oceanic convergence variance explained by each variable. Variances explained in parentheses for the Southern, Arctic and Irminger temperature fluxes indicate the sensitivity to the choice of θ_{ref} (time-mean volume-average, climatological mean volume-average). Variances explained >50% are shown in bold.

We also use two terms to refer to the oceanic fluxes. When mass is conserved, we refer to the oceanic fluxes as heat fluxes, as these are unchanged by the reference temperature. When mass is not conserved, we refer to the oceanic fluxes as temperature fluxes, as these are sensitive to the reference temperature.

3. Heat Budget of the Eastern SPG

To analyze the heat budget of the eastern SPG, we use the following equations:

$$\frac{\mathrm{dOHC}}{\mathrm{dt}} = Q_{\mathrm{oce}} + Q_{\mathrm{sfc}}$$

$$Q_{\mathrm{oce}} = \rho_0 * C_{\mathrm{p}} * \left[\oint_{\mathrm{Sou}} \int_{z_{\mathrm{bot}}}^{z_{\mathrm{sfc}}} \vec{u}(\theta - \theta_{\mathrm{ref}})\, \mathrm{dz\, dl} + \oint_{\mathrm{Arc}} \int_{z_{\mathrm{bot}}}^{z_{\mathrm{sfc}}} \vec{u}(\theta - \theta_{\mathrm{ref}})\, \mathrm{dz\, dl} + \oint_{\mathrm{Irm}} \int_{z_{\mathrm{bot}}}^{z_{\mathrm{sfc}}} \vec{u}(\theta - \theta_{\mathrm{ref}})\, \mathrm{dz\, dl} \right]$$

where the temporal derivative of OHC has units of J/s or W; Q_{oce} is the convergence of ocean heat fluxes (positive inward); Q_{sfc} is the sum of the latent, sensible, shortwave, and longwave flux (units = W, positive downward); t is time (units = s); ρ_0 is a reference density (1,029 kg/m^3); C_p is the specific heat of seawater (3,994 J · kg^{-1} · K^{-1}); $\vec{u}$ is the velocity normal to each face of the spatial domain (units = m/s, positive inward); θ is potential temperature (units = K); θ_{ref} is the mean potential temperature of the region (units = K); z is depth (units = m); l is along-face distance (units = m); and subscripts Sou, Arc and Irm refer to each face of our domain. Comparison of the temperature fluxes to the total ocean heat divergence requires defining a reference temperature. Here we choose to follow the methods described in Lee et al. (2004) to reference the temperature fluxes to the time-varying, volume-averaged temperature of the region, θ_{ref}, because it gives a physically relevant context to assess OHC changes; a flux into the region of colder (warmer) than average water results in a cooling (warming) of the region. The magnitude of the temperature flux depends on the mean temperature of the region thus these temperature fluxes should only be compared to each other, rather than to basin-scale observations such as from RAPID (Johns et al., 2011) or OSNAP (Lozier et al., 2017). We also compute the temperature fluxes with two other choices of a physically relevant reference temperature (time-mean volume-averaged temperature and climatological mean volume-averaged temperature) and find that the relative contributions of ocean and surface forcing to OHC variability are unchanged. The choice of reference temperature does impact the relative contribution of the flux across each face to OHC variability (see Table 1), but the differences are sufficiently small to not impact our study conclusions, thus we present results here based on the reference temperature recommended by Lee et al. (2004).

In both models, a time-mean net ocean heat flux convergence in the region is balanced by ocean heat loss to the atmosphere (Table 1 and Figure S1). The net advective ocean heat flux convergence (0.11 PW in FLAME and 0.09 PW in ECCO) is achieved by a positive temperature flux through the southern face that is only partially compensated by the smaller and negative temperature fluxes through the Arctic and Irminger faces.

An investigation of the temporally varying OHC reveals that surface forcing dominates the OHC tendency on seasonal time scales (Table 1, left columns), while the total oceanic convergence is of secondary importance. In the exploration of interannual variability (when the monthly means have been removed; Table 1, right columns), the relative roles of surface forcing and oceanic convergence change. In FLAME, the oceanic heat flux convergence explains 80% of the OHC tendency as opposed to 16% on seasonal time scales. Of the oceanic fluxes, the flux through the Southern face is the most important. Thus, in FLAME at interannual time scales, the flux through the Southern face is the primary control on OHC tendency, with the surface forcing playing a secondary role.

In ECCO, the surface forcing remains as important to OHC tendency as the ocean heat flux divergence even after the removal of the seasonal cycle. One possible explanation for the discrepancy between the models (that ECCO shows a higher contribution from the surface fluxes than FLAME at these time scales) is the difference in time periods covered. It has already been established that the strong warming in the winter of 1995/1996 was driven by ocean heat convergence (Barrier et al., 2015; Grist et al., 2010), while the strong cooling in the winters of 2013/2014 and 2014/2015 was driven by surface forcing (Josey et al., 2018). However, an examination of the overlapping period between FLAME and ECCO (1992–2004) reveals that surface forcing still explains 66% of the OHC tendency in ECCO (as opposed to 37% in FLAME). Another possibility is that the surface forcing in ECCO is considerably stronger than in FLAME. We find that while the means are very similar, the variance of the ECCO surface fluxes (adjusted from ERA-Interim, standard deviation = 38.8 TW) is considerably higher than the FLAME surface fluxes (NCEP/NCAR anomalies, standard deviation = 28.3 TW). Thus, the stronger variability in ECCO surface flux fields likely explains the stronger connection between the OHC tendency and the surface fluxes in ECCO than in FLAME. Finally, we also posit that the difference in the resolution of the models (ECCO = 1/4–1° and FLAME = 1/12°) could lead to ECCO underestimating the oceanic eddy heat fluxes, a process that has recently been shown to be important in this region from observations (Zhao et al., 2018) and in FLAME at the inter-gyre latitudes (Figure S2).

4. Origins of Variability in Southern Flux

4.1. Eulerian Meridional Heat Transport

To determine the origin of variability in the temperature flux through the Southern face, we first examine the meridional coherence of the Atlantic meridional heat transport (MHT; Figures 2a and S2). MHT is calculated as

$$\mathrm{MHT}(\phi, \mathrm{t}) = \rho_0 * \mathrm{C_p} * \iint \overrightarrow{v}(\lambda, \phi, z, t)\theta(\lambda, \phi, z, t)\, d\lambda\, dz$$

where ϕ is latitude (units = m), $\overrightarrow{v}$ is the meridional velocity (units = m/s), and λ is longitude (units = m). There is a distinct break in the meridional coherence (Figure 2a) at the intergyre latitudes (35–40°N), which has been previously reported in the AMOC (Bingham et al., 2007; Lozier et al., 2010) and Atlantic MHT (Kelly et al., 2014). The range of latitudes with positive correlations is limited to within the STG (15–40°N) and within the SPG (45–63°N), while the correlations between the two gyres are largely negative. This cross-latitudinal plot shows that a single measure of the Atlantic MHT is not representative of the entire basin. Thus, the origin of MHT anomalies in the SPG (e.g., the large heat convergence and subsequent warming in the winter of 1995/1996) and in particular whether the anomalies are propagating meridionally is not readily apparent from this basin-scale, Eulerian perspective.

4.2. Backward Lagrangian Trajectories

We next perform a Lagrangian experiment to determine the origin of the newly arrived waters to the eastern SPG. In FLAME, we seed all northward flowing water along the Southern face (54.5°N, 35°-9°W, 0–500 m) with trajectories every 30 days and run the trajectories backward in time through the three-dimensional velocity field for 5 years (Figure 2b). The number of trajectories initialized in each grid cell at each time step is proportional to the volume transport through each grid cell (0.01 Sv per trajectory). This launch strategy allows the

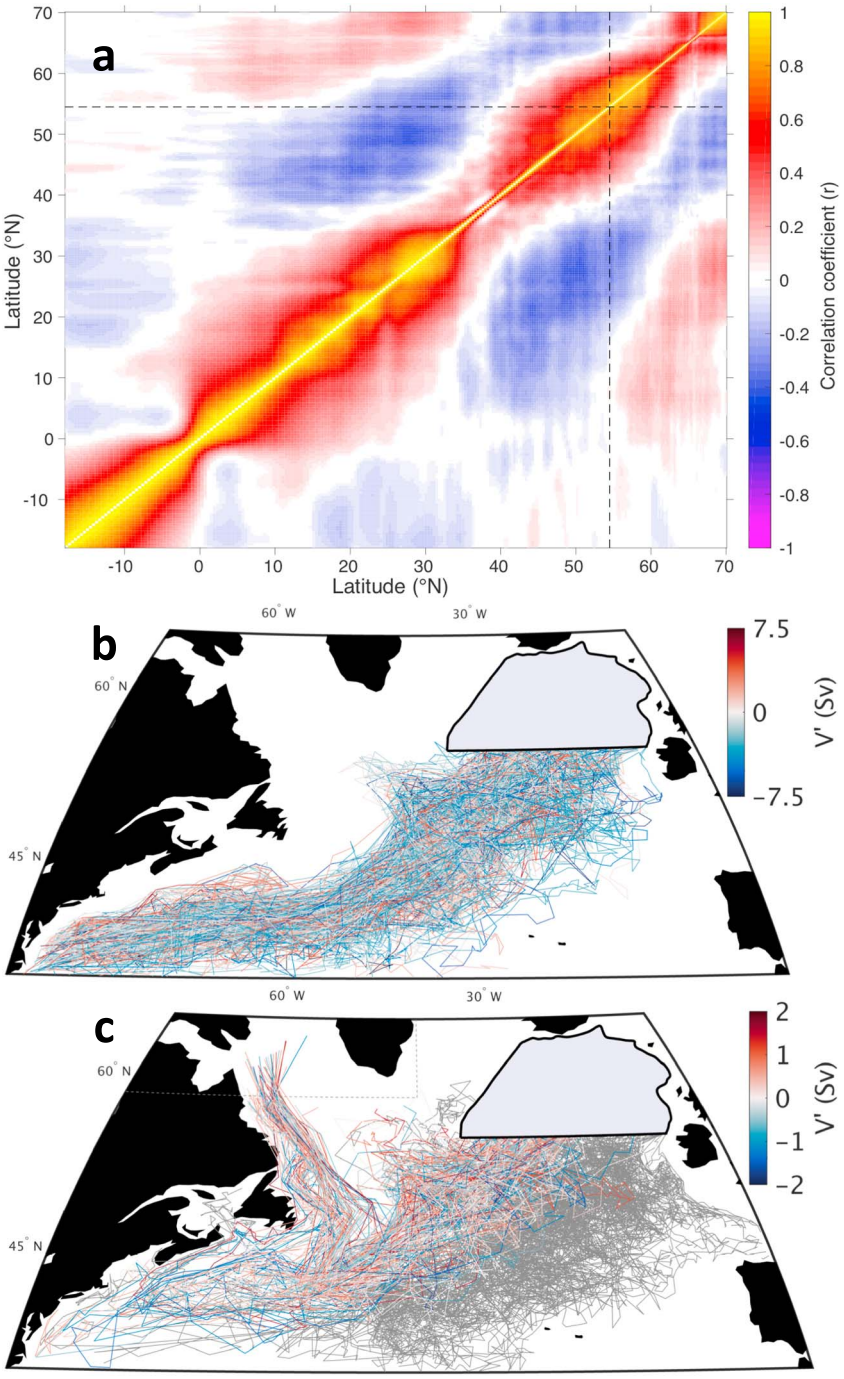

Figure 2. Eulerian and Lagrangian perspectives in FLAME on intergyre heat transport. (a) The correlation of MHT between latitudes shows a positive intragyre correlation and negative inter-gyre correlations. The black dashed lines at 54.5°N mark the southern face latitude. (b and c) Lagrangian trajectories divided into four groups: STG origin (colored by transport anomaly at initialization in panel b, 43% of total, 17.5 ± 3.3 Sv, 0.31 ± 0.07 PW), western SPG-origin (colored by transport anomaly at initialization in panel c, 8% of total, 3.1 ± 0.69 Sv, 0.04 ± 0.01 PW), trajectories that do not cross any line within 5 years (gray in panel c, 10% of total, 4.1 ± 0.74 Sv, 0.06 ± 0.01 PW), and trajectories that recirculate across the Southern face (not shown, 39% of total, 0.24 ± 0.07 PW). The box (gray dashed at 58°N and 40°W) in panel c is used to define the western SPG. The maps' southern boundary at 35°N is used to define the subtropical gyre.

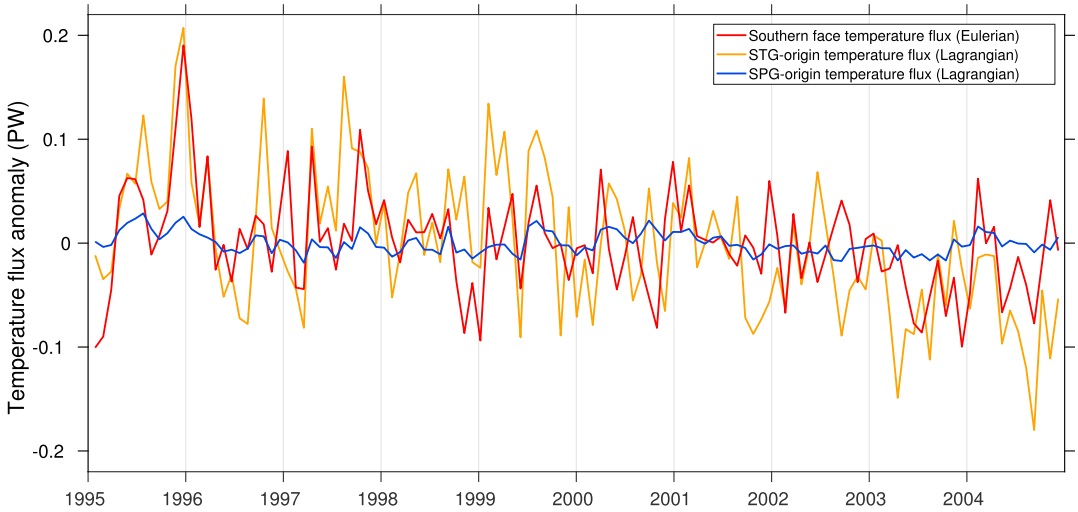

Figure 3. A comparison in FLAME between the Eulerian temperature flux through the Southern face (red), the Lagrangian-derived subtropical gyre-origin temperature flux (yellow), and the Lagrangian-derived subpolar-origin temperature flux (blue). Note that the Lagrangian time series start in 1995 because the trajectories are given 5 years to reach their respective destinations.

Lagrangian trajectories to be readily converted to Sverdrups of volume transport and then used in the calculation of a temperature flux. We then divide the trajectories based on their location of origin.

On monthly time scales, the subtropical-origin temperature flux across the Southern face (Figure 3, yellow) explains 22% of the total temperature flux through the Southern face (red), and the SPG-origin temperature flux (blue) explains 16% of the total. This (relatively weak) relationship between the Eulerian Southern flux and the Lagrangian subtropical-origin temperature flux seems to be wholly driven by the large anomaly in December of 1995, which dominates the time series during this 15-year period. If 1995 is excluded, the subtropical-origin temperature flux explains only 10% of the Southern flux variability and the subpolar-origin temperature flux explains 13%. When the time series are low-passed filtered with a 13-month running-mean, the subtropical influence becomes dominant regardless of the period covered: the STG-origin flux explains 60% of the Southern flux for the whole 1995–2004 period, and 53% post-1995, while the SPG-origin flux explains only 22% for the whole period, and 13% post-1995. The other two groups of trajectories explain negligible amounts of the variance at all frequencies. Thus, the Lagrangian-derived subtropical influence explains the majority of interannual variability in the Eulerian temperature flux through the Southern face.

Finally, the subtropical-origin temperature flux variability is primarily driven by transport variability ($r = 0.94$) with a secondary role from temperature variability ($r = 0.59$), in line with previous results on the relative roles of anomalous temperature and anomalous transport to the heat fluxes in this region (Foukal & Lozier, 2016; Gary et al., 2018). This result shows that the strength of the inter-gyre connection from the STG to the SPG is an important contributor to the temperature flux through the Southern face.

This Lagrangian result supports the AMOC explanation of SPG OHC variability from Robson et al. (2016) rather than the horizontal gyre explanation from Piecuch et al. (2017) because we find that the eastern SPG OHC variability on interannual time scales is mainly driven by variability sourced in the subtropics. In support of this result, a Eulerian decomposition of the total MHT in density space at 54.5°N (Figure S3), which is the southern boundary of our study domain, reveals that overturning dynamics can explain 82% of the total MHT variance, while gyre dynamics explain 45%. Thus, from both the Lagrangian and Eulerian perspectives, the waters carried in the upper limb of the AMOC appear to play a large role in setting the interannual OHC variability in the eastern subpolar North Atlantic, a region where this influence is likely maximized. Finally, we note that Piecuch et al. (2017) and others (e.g., Williams et al., 2014) use depth coordinates for the decomposition of the MHT in the subpolar North Atlantic, and as such likely underestimate the contribution of overturning dynamics to MHT variability in the subpolar North Atlantic. As has been demonstrated in past studies, it is more appropriate to define the AMOC in density space at subpolar latitudes (Holliday et al., 2018;

Kwon & Frankignoul, 2014; Lherminier et al., 2007; Xu et al., 2016), which are characterized by strongly zonally-sloped isopycnals.

5. Conclusions

We draw four conclusions:

1. In both FLAME and ECCO, the surface forcing (latent + sensible + shortwave + long-wave) exerts the primary control on eastern SPG OHC variability on seasonal time scales, explaining 90–94% of OHC tendency (Table 1).
2. When the seasonal cycle is removed, the ocean heat flux divergence becomes as important (ECCO) or more important (FLAME) than the surface forcing.
3. The temperature flux through the southern face of our study area is the dominant component of the ocean heat flux divergence on seasonal to interannual time scales.
4. On interannual time scales, the temperature flux through the Southern face of our study area can be largely explained by variability in the strength of the intergyre throughput, which is effectively the upper limb of the overturning circulation.

Acknowledgments
We would like to thank Mark Cane and one anonymous reviewer for insightful comments that significantly improved the manuscript. We would also like to thank Claus Böning and Arne Biastoch (GEOMAR) for the FLAME data, as well as Stefan Gary for tailoring the B-grid Lagrangian trajectory code to our lab's needs. FLAME data used to create the figures are available at the following DOI: 10.7924/r4zw1d509. Other data used in this work are available from the MetOffice EN4 website (http://www.metoffice.gov.uk/hadobs/en4/) and the ECCO website (https://ecco.jpl.nasa.gov/products/latest/), with special thanks to Ou Wang from NASA JPL. This work has benefitted from discussions with Bill Johns, Nicolas Cassar, Paul Baker, Sijia Zou, Ryan Peabody, Kim Drouin, Feili Li, and Laifang Li. This work was supported by the NASA Earth and Space Sciences Graduate Fellowship (NNX13AO21H) and the NSF Physical Oceanography Program (NSF-OCE-12-59102; awarded to MSL). The authors do not report any conflicts of interest.

References

Alheit, J., Licandro, P., Coombs, S., Garcia, A., Giráldez, A., Garcia Santamaría, M. T., et al. (2017). Atlantic Multidecadal Oscillation (AMO) modulates dynamics of small pelagic fishes and ecosystem regime shifts in the eastern North and Central. *Atlantica*, *131*, 21–25.

Årthun, M., Kolstad, E. W., Eldevik, T., & Keenlyside, N. (2018). Time scales and sources of European temperature variability. *Geophysical Research Letters*, *45*, 3597–3604. https://doi.org/10.1002/2018GL077401

Barrier, N., Deshayes, J., Treguier, A.-M., & Cassou, C. (2015). Heat budget in the North Atlantic subpolar gyre: Impacts of atmospheric weather regimes on the 1995 warming event. *Progress in Oceanography*, *130*, 75–90. https://doi.org/10.1016/j.pocean.2014.10.001

Bellomo, K., Murhpy, L. M., Cane, M. A., Clement, A. C., & Polvani, L. M. (2017). Historical forcings as main drivers of the Atlantic multidecadal oscillation in the CESM large ensemble. *Climate Dynamics*, *50*(9-10), 3687–3698. https://doi.org/10.1007/s00382-017-3834-3

Biastoch, A., Böning, C. W., Getzlaff, J., Molines, J. –. J., & Madec, G. (2008). Causes of interannual-decadal variability in the meridional overturning circulation of the Midlatitude North Atlantic Ocean. *Journal of Climate*, *21*(24), 6599–6615. https://doi.org/10.1175/2008JCLI2404.1

Bingham, R. J., Hughes, C. W., Roussenov, V., & Williams, R. G. (2007). Meridional coherence of the North Atlantic meridional overturning circulation. *Geophysical Research Letters*, *34*, L23606. https://doi.org/10.1029/2007GL031731

Boccaletti, G., Ferrari, R., Adcroft, A., Ferreira, D., & Marshall, J. (2005). The vertical structure of ocean heat transport. *Geophysical Research Letters*, *32*, L10603. https://doi.org/10.1029/2005GL022474

Böning, C. W., Scheinert, M., Dengg, J., Biastoch, A., & Funk, A. (2006). Decadal variability of subpolar gyre transport and its reverberation in the North Atlantic overturning. *Geophysical Research Letters*, *33*, L21S01. https://doi.org/10.1029/2006GL026906

Bower, A. S., Le Cann, B., Rossby, T., Zenk, W., Gould, J., Speer, K., et al. (2002). Directly measured mid-depth circulation in the northeastern North Atlantic Ocean. *Nature*, *419*(6907), 603–607. https://doi.org/10.1038/nature01078

Brown, P. B., Lozier, M. S., Zhang, R., & Li, W. (2016). The necessity of cloud feedback for a basin-scale Atlantic multidecadal oscillation. *Geophysical Research Letters*, *43*, 3955–3963. https://doi.org/10.1002/2016GL068303

Buckley, M. W., Ferreira, D., Campin, J.-M., Marshall, J., & Tulloch, R. (2012). On the relationship between decadal buoyancy anomalies and variability of the Atlantic Meridional Overturning Circulation. *Journal of Climate*, *25*, 8009–8030. https://doi.org/10.1175/JCLI-D-11-00505.1

Burkholder, K. C., & Lozier, M. S. (2014). Tracing the pathways of the upper limb of the North Atlantic Meridional Overturning Circulation. *Geophysical Research Letters*, *41*, 4254–4260. https://doi.org/10.1002/2014GL060226

Cane, M. A., Clement, A. C., Murphy, L. M., & Bellomo, K. (2017). Low pass filtering, heat flux and Atlantic multidecadal variability. *Journal of Climate*, *30*(18), 7529–7553. https://doi.org/10.1175/JCLI-D-16-0810.1

Clement, A., Bellomo, K., Murphy, L. N., Cane, M. A., Mauritsen, T., Radel, G., & Stevens, B. (2015). The Atlantic multidecadal oscillation without a role for ocean circulation. *Science*, *350*(6258), 320–324. https://doi.org/10.1126/science.aab3980

Delworth, T. L., Zeng, F., Zhang, L., Zhang, R., Vecchi, G. A., & Yang, X. (2017). The central role of ocean dynamics in connecting the North Atlantic Oscillation to the extratropical component of the Atlantic Multidecadal Oscillation. *Journal of Climate*, *30*(10), 3789–3805. https://doi.org/10.1175/JCLI-D-16-0358.1

Desbruyères, D., Mercier, H., & Thierry, V. (2015). On the mechanisms behind decadal heat content changes in the eastern subpolar gyre. *Progress in Oceanography*, *132*, 262–272. https://doi.org/10.1016/j.pocean.2014.02.005

Desbruyères, D., Thierry, V., & Mercier, H. (2013). Simulated decadal variability of the meridional overturning circulation across the A25-Ovide section. *Journal of Geophysical Research: Oceans*, *118*, 462–475. https://doi.org/10.1029/2012JC008342

Forget, G., Campin, J. M., Heimbach, P., Hill, C. N., Ponte, R. M., & Wunsch, C. (2015). ECCO version 4: An integrated framework for non-linear inverse modeling and global ocean state estimation. *Geoscientific Model Development Discussion*, *8*(5), 3653–3743. https://doi.org/10.5194/gmdd-8-3653-2015

Foukal, N. P., & Lozier, M. S. (2016). No inter-gyre pathway for sea-surface temperature anomalies in the North Atlantic. *Nature Communications*, *7*, 11333. https://doi.org/10.1038/ncomms11333

Foukal, N. P., & Lozier, M. S. (2017). Assessing variability in the size and strength of the North Atlantic subpolar gyre. *Journal of Geophysical Research: Oceans*, *122*, 6295–6308. https://doi.org/10.1002/2017JC012798

Frajka-Williams, E., Beaulieu, C., & Duchez, A. (2017). Emerging negative Atlantic multidecadal oscillation index in spite of warm subtropics. *Scientific Reports*, *7*(1), 11224. https://doi.org/10.1038/s41598-017-11046.

Fukumori, I., Wang, O., Fenty, I., Forget, G., Heimbach, P., & Ponte, R. (2017). ECCO Version 4 Release. Retrieved from http://hdl.handle.net/1721.1/110380, doi:1721.1/110380, ftp://ecco.jpl.nasa.gov/Version4/Release3/doc/v4r3_estimation_synopsis.pdf

Gary, S. F., Cunningham, S. A., Johnson, C., Houpert, L., Holliday, N. P., Behrens, E., et al. (2018). Seasonal cycles of oceanic transports in the eastern subpolar North Atlantic. *Journal of Geophysical Research: Oceans*, *123*, 1471–1484. https://doi.org/10.1002/2017JC013350

Gary, S. F., Lozier, M. S., Böning, C. W., & Biastoch, A. (2011). Deciphering the pathways for the deep limb of the Meridional Overturning Circulation. *Deep Sea Research, Part II*, *58*(17-18), 1781–1797. https://doi.org/10.1016/j.dsr2.2010.10.059

Good, S. A., Martin, M. J., & Rayner, N. A. (2013). EN4: Quality controlled ocean temperature and salinity profiles and monthly objective analysis with uncertainty estimates. *Journal of Geophysical Research: Oceans*, *118*, 6704–6716. https://doi.org/10.1002/2013JC009067

Grist, J., Josey, S. A., Marsh, R., Good, S. A., Coward, A. C., de Cuevas, B. A., et al. (2010). The roles of surface heat flux and ocean heat transport convergence in determining Atlantic Ocean temperature variability. *Ocean Dynamics*, *60*(4), 771–790. https://doi.org/10.1007/s10236-010-0292-4

Häkkinen, S., & Rhines, P. (2004). Decline of subpolar North Atlantic circulation during the 1990s. *Science*, *304*(5670), 555–559. https://doi.org/10.1126/science.1094917

Hátún, H., Payne, M. R., & Jacobsen, J. A. (2009). The North Atlantic subpolar gyre regulates the spawning distribution of blue whiting (Micromesistius poutassou). *Canadian Journal of Fisheries and Aquatic Sciences*, *66*(5), 759–770. https://doi.org/10.1139/F09-037

Hátún, H., Sandø, A. B., Drange, H., Hansen, B., & Valdimarsson, H. (2005). Influence of the Atlantic subpolar gyre on the thermohaline circulation. *Science*, *309*(5742), 1841–1844. https://doi.org/10.1126/science.1114777

Holliday, N. P. (2003). Air-sea interaction and circulation changes in the Northeast Atlantic. *Journal of Geophysical Research*, *108*(C8), 3259. https://doi.org/10.1029/2002JC001344

Holliday, N. P., Bacon, S., Cunningham, S. A., Gary, S. F., Karstensen, J., King, B. A., et al. (2018). Subpolar North Atlantic overturning and gyre-scale circulation in the summers of 2014 and 2016. *Journal of Geophysical Research: Oceans*, *123*, 4538–4559. https://doi.org/10.1029/2018JC013841

Johns, W. E., Baringer, M. O., Beal, L. M., Cunningham, S. A., Kanzow, T., Bryden, H. L., et al. (2011). Continuous, array-based estimates of Atlantic Ocean heat transport at 26.5°N. *Journal of Climate*, *24*(10), 2429–2449. https://doi.org/10.1175/2010JCLI3997.1

Josey, S. A., Hirschi, J. J. M., Sinha, B., Duchez, A., Grist, J. P., & Marsh, R. (2018). The recent Atlantic cold anomaly: Causes, consequences, and related phenomena. *Annual Review of Marine Science*, *10*(1), 475–501. https://doi.org/10.1146/annurev-marine-121916-063102

Kalnay, E., Kanamitsu, M., Kistler, R., Collins, W., Deaven, D., Gandin, L., et al. (1996). The NCEP/NCAR 40-year reanalysis project. *Bulletin of the American Meteorological Society*, *77*(3), 437–471. https://doi.org/10.1175/1520-0477(1996)077<0437:TNYRP>2.0.CO;2

Kelly, K. A., Thompson, L., & Lyman, J. (2014). The coherence and impact of meridional heat transport anomalies in the Atlantic Ocean inferred from observations. *Journal of Climate*, *27*(4), 1469–1487. https://doi.org/10.1175/JCLI-D-12-00131.1

Kwon, Y.-O., & Frankignoul, C. (2014). Mechansisms of multidecadal Atlantic meridional overturning circulation variability diagnosed in depth versus density space. *Journal of Climate*, *27*(24), 9359–9376. https://doi.org/10.1175/JCLI-D-14-00228.1

Latif, M., Collins, M., Pohlmann, H., & Keenlyside, N. (2006). A review of predictability studies of Atlantic sector climate on decadal time scales. *Journal of Climate – Special Edition*, *19*(23), 5971–5987. https://doi.org/10.1175/JCLI3945.1

Lee, T., Fukumori, I., & Tang, B. (2004). Temperature advection: Internal versus external processes. *Journal of Physical Oceanography*, *34*(8), 1936–1944. https://doi.org/10.1175/1520-0485(2004)034<1936:TAIVEP>2.0.CO;2

Lherminier, P., Mercier, H., Gourcuff, C., Alvarez, M., Bacon, S., & Kermabon, C. (2007). Transports across the 2002 Greenland-Portugal Ovide section and comparison with 1997. *Journal of Geophysical Research*, *112*, C07003. https://doi.org/10.1029/2006JC003716

Lozier, M. S., Bacon, S., Bower, A. S., Cunningham, S. A., Femke de Jong, M., de Steur, L., et al. (2017). Overturning in the subpolar North Atlantic program: A new international ocean observing system. *Bulletin of the American Meteorological Society*, *98*(4), 737–752. https://doi.org/10.1175/BAMS-D-16-0057.1

Lozier, M. S., Roussenov, V., Reed, M. S. C., & Williams, R. G. (2010). Opposing decadal changes for the North Atlantic meridional overturning circulation. *Nature Geoscience*, *3*(10), 728–734. https://doi.org/10.1038/ngeo947

Murphy, L. N., Bellomo, K., Cane, M., & Clement, A. (2017). The role of historical forcings in simulating the observed Atlantic multidecadal oscillation. *Geophysical Research Letters, 44*, 2472-2480. https://doi.org/10.1002/2016GL071337

Pacanowski, R. C. (1996). MOM 2 documentation user's guide and reference manual, Geophysical Fluid Dynamics Laboratory Ocean Technical Report 3.2 GFDL/NOAA, Princeton.

Piecuch, C. G. (2017). A Note on Practical Evaluation of Budgets in ECCO Version 4 Release 3.

Piecuch, C. G., Ponte, R. M., Little, C. M., Buckley, M. W., & Fukumori, I. (2017). Mechanisms underlying recent decadal changes in subpolar North Atlantic Ocean heat content. *Journal of Geophysical Research: Oceans*, *122*, 7181–7197. https://doi.org/10.1002/2017JC012845

Rahmstorf, S., Box, J. E., Feulner, G., Mann, M. E., Robinson, A., Rutherford, S., & Schaffernicht, E. J. (2015). Exceptional twentieth-century slowdown in Atlantic Ocean overturning circulation. *Nature Climate Change*, *5*(5), 475–480. https://doi.org/10.1038/nclimate2554

Roberts, C. D., Palmer, M. D., Allan, R. P., Desbruyères, D. G., Hyder, P., Liu, C., & Smith, D. (2017). Surface flux and ocean heat transport convergence contributions to seasonal and interannual variations of ocean heat content. *Journal of Geophysical Research: Oceans*, *122*, 726–744. https://doi.org/10.1002/2016JC012278

Robson, J., Ortega, P., & Sutton, R. (2016). A reversal of climatic trends in the North Atlantic since 2005. *Nature Geoscience*, *9*(7), 513–517. https://doi.org/10.1038/NGEO2727

Sutton, R. T., & Allen, M. R. (1997). Decadal predictability of North Atlantic Sea surface temperature and climate. *Nature*, *388*(6642), 563–567. https://doi.org/10.1038/41523

Trenary, L., & DelSole, T. (2016). Does the Atlantic multidecadal oscillation get its predictability from the Atlantic Meridional Overturning circulation? *Journal of Climate*, *29*(14), 5267–5280. https://doi.org/10.1175/JCLI-D-16-0030.1

Williams, R. G., Roussenov, V., Smith, D., & Lozier, M. S. (2014). Decadal evolution of ocean thermal anomalies in the North Atlantic: The effects of Ekman, overturning and horizontal transport. *Journal of Climate*, *27*(2), 698–719. https://doi.org/10.1175/JCLI-D-12-00234.1

Xu, X., Rhines, P. B., & Chassignet, E. P. (2016). Temperature-salinity structure of the North Atlantic circulation and associated heat and freshwater transports. *Journal of Climate*, *29*(21), 7723–7742. https://doi.org/10.1175/JCLI-D-15-0798.1

Zhao, J., Bower, A., Yang, J., & Lin, X. (2018). Meridional heat transport variability induced by mesoscale processes in the subpolar North Atlantic. *Nature Communications*, *9*(1), 1124. https://doi.org/10.1038/s41467-018093134-x